J Nanostruct 13(4): 978-988, Autumn 2023

RESEARCH PAPER

Synthesis and Antibacterial Activity of ZnO Nanoparticle Coatings for Titanium Orthodontic Fixed Retainers

Shahbaa A. Mohammed [1], *Mohammed Nahidh* [1], *Mohammed K. Khalaf* [2] *

[1] *Orthodontic Department, College of Dentistry, University of Baghdad, Baghdad, Iraq*

[2] *Authority of Scientific Research, Ministry of Higher Education and Scientific Research, Baghdad, Iraq*

ARTICLE INFO

Article History:
Received 23 July 2023
Accepted 17 September 2023
Published 01 October 2023

Keywords:
Antibacterial Nanocoatings
Electrophoretic deposition
Orthodontic Fixed Retainers
Surface morphology
Zinc oxide

ABSTRACT

This study delves into the utilization of cathodic electrophoretic deposition (EPD) as a technique for the application of zinc oxide (ZnO) nanostructured films onto substrates made of Ti6Al4V alloy within an aqueous environment. The primary focus was to investigate the structural and topographical attributes of the coated films. These characteristics were meticulously examined using X-ray Diffractometry (XRD) and Atomic Force Microscopy (AFM). A significant aspect of this research was the assessment of the antibacterial efficacy of these nanoparticle-coated films, particularly for their potential use in orthodontic fixed retainers. The experimental process involved the creation of films with varying properties by altering the concentrations of ZnO nanoparticles (2, 3, 4, 5 gm), the applied voltages (10, 30, 50 Volt), and the spacing between the electrodes (1, 3, 5 cm). A notable observation was the correlation between the increase in coating mass and the applied voltage. The crystalline size of the films was consistently below 50nm, and an increase in surface roughness was observed in proportion to the voltage applied. The antibacterial properties of the EPD-deposited ZnO films were particularly noteworthy. Extensive testing revealed a high level of antibacterial activity against pathogens such as *Streptococcus mutans*, *Lactobacillus*, and *Candida albicans*. These findings highlight the potential of using ZnO/Ti6Al4V composite structures in orthodontic applications, specifically for fixed retainers, due to their effective antibacterial properties and the controlled nanostructuring achievable through EPD.

How to cite this article
Mohammed S A., Nahidh M., Khalaf M K. Synthesis and Antibacterial Activity of ZnO Nanoparticle Coatings for Titanium Orthodontic Fixed Retainers. J Nanostruct, 2023; 13(4):978-988. DOI: 10.22052/JNS.2023.04.007

INTRODUCTION

Oral hygiene becomes notably intricate after the placement of fixed orthodontic appliances. In a considerable number of patients undergoing fixed orthodontic treatment, these fixed appliances remain in use throughout the treatment duration, typically spanning 1.5 to 2 years [1,2]. Both the brackets and the adhesive materials employed for bonding may retain plaque, introducing a susceptibility to dental caries at this newly established site. This susceptibility arises due to a significant elevation in the levels of *Streptococcus mutans* detected in both saliva and plaque among patients undergoing fixed orthodontic appliance treatment [3]. Consequently, this situation escalates the risk of dental caries.

* *Corresponding Author Email: mohammedkhkh@yahoo.com*

To address these issues and to enhance the performance of orthopedic and dental implants, coatings comprising organic and inorganic materials are applied to dental appliances. These coatings serve the dual purposes of ensuring biocompatibility, resistance against inflammation, and demonstrating antibacterial properties. Among the inorganic coatings considered for this purpose are metal oxides such as ZnO, TiO_2, ZrO_2, Nb_2O_5, and Ta_2O_5 [4,5].

To further enhance the antibacterial, bone regeneration, and cohesion properties of bone implants, employing zinc oxide (ZnO) nanoparticle films as coatings is an exemplary choice [6]. The United States Federal Drug Administration has categorized ZnO as generally recognized as safe (GRAS), as per 21CFR182.8991 [7]. This can be achieved with both naturally occurring substances and those purposefully developed for their nanoscale properties [8]. Nonetheless, there is a scarcity of comprehensive research studies that have systematically characterized ZnO nanoparticles coated on Ti6Al4V alloy samples, particularly concerning their suitability for orthodontic fixed retainers. Existing literature reveals that ZnO coatings can be fabricated using various methods, including chemical vapor deposition, radio frequency magnetron sputtering, molecular beam epitaxy, sol-gel processes, hydrothermal synthesis, and electrochemical or electrophoretic deposition [9-15]. The technique of electrophoretic deposition (EPD) represents a cost-effective method for the production of highly uniform films, characterized by thickness ranging from the nanometer to micrometer scale. This uniformity is achieved by manipulating the applied voltage and deposition time. The key advantages associated with the EPD method encompass the following aspects [16,17]: its applicability to any solid material available in a finely powdered form, its capacity for rapid film deposition, cost-effectiveness, straightforward instrumentation, minimal restrictions concerning substrate shapes, and resource conservation.

EPD has gained prominence as a valuable technique for the creation of nanostructured ZnO films[17-26]. It is noteworthy that both aqueous and non-aqueous ZnO suspensions have been effectively employed to coat a wide array of substrates, including transparent conductive oxide glass, anodic alumina membranes, as well as steel, nickel, and titanium. In the context of depositing ZnO coatings on Ti6Al4V substrates, the electrophoretic coating technique has been chosen for its capacity to afford control over parameters such as coating thickness, chemical composition, and particle sizes [27,28]. The primary objective of this scholarly investigation is to rigorously examine the effects and implications of zinc oxide (ZnO) coatings, applied onto Ti6Al4V alloy substrates using the cathodic electrophoretic deposition (EPD) technique. This study aims to meticulously characterize and analyze the resultant surface properties utilizing advanced methodologies such as X-ray Diffraction (XRD) and Atomic Force Microscopy (AFM). Moreover, a significant aspect of this research is dedicated to evaluating the antimicrobial efficacy of the ZnO nanoparticle-coated Ti6Al4V alloy surfaces, specifically in the context of their application in orthodontic devices. This comprehensive analysis is poised to contribute valuable insights into the potential of ZnO coatings in enhancing the functional and hygienic properties of orthodontic materials.

MATERIALS AND METHODS

The ASTM Grade 5 titanium alloy, also known as Ti_6Al_4V, was procured from BAOJI JINSHENG METAL MATERIAL CO., LTD. The alloy composition consists of titanium (Ti) at 90%, aluminum (Al) at 6%, and vanadium (V) at 4%. It falls under the category of alpha-beta titanium alloys, with aluminum serving to stabilize the alpha phase and vanadium contributing to the stabilization of the beta phase. Ti6Al4V is widely favored due to its exceptional combination of material properties. It can undergo further processing to tailor its attributes for specific applications. Upon receipt of the alloy in sheet form for electrophoretic deposition, the samples were prepared by employing a cutting machine with a slow cutting speed. A cutting fluid was also employed to prevent the generation of excessive heat during the cutting process. The sample dimensions were determined in accordance with the required tests: samples measuring 2x10x20 mm for characterization and disc-shaped samples with a diameter of 6 mm for the antimicrobial diffusion test. The Ti6Al4V alloy samples were smoothed using silicon carbide-based smoothing paper with a granular size of 500 microns. Subsequently, they were subjected to chemical cleaning with a solution comprising oxygen (O_2), hydrofluoric acid (HF), and nitric acid

(H_3HNO) in volume ratios of 3:1:6, respectively. The samples underwent a thorough washing process using 90% ethanol in an ultrasound bath for 10 minutes, repeated twice, followed by a final wash using distilled water in an ultrasound bath for an additional 10 minutes.

For the electrophoretic deposition process, a solution was prepared containing nano-sized ZnO particles (ranging from 2 to 5 g), 100 ml of 90% ethanol, and 2 g of Polyvinylpyrrolidone (PVP) binder. In this process, the Ti6Al4V samples served as the cathode, while a graphite electrode was employed as the anode. These electrodes were connected to a power supply, with varying electrode distances (1, 3, and 5 cm) and voltage settings (10, 30, and 50 Volts) applied for a duration of 5 minutes. Following deposition, the samples were air-dried for 1 hour. X-ray diffraction (XRD) measurements were carried out using a Shimadzu X-ray diffractometer with a wavelength of 1.54056 Å. Surface morphology analysis was conducted using an Atomic Force Microscope (NaioAFM, Switzerland). In accordance with Standard ISO 20645:2004 (BS EN ISO 20645:2004 or GB/T 20944.1), antimicrobial testing was performed utilizing Mueller Hinton agar for diffusion tests. Disc-shaped coated specimens measuring 6 mm in diameter and 2 mm in thickness were employed for this examination, following the guidelines of the Clinical and Laboratory Standards Institute (CLSI; 2018).

The density of test cultures was adjusted to an optimal value of 0.5 McFarland standards (equivalent to 1.5×10^8 CFU/mL) for the antibacterial assays. Coated and uncoated specimens were systematically placed in the culture at specific millimeter intervals. Each test plate accommodated three samples, with a total of 10 samples for each group (control and optimized EPD). The plates were incubated at 37°C for 24-48 hours. The assessment of antibacterial activity was based on the measurement of the width of an inhibition zone (H) surrounding the samples, calculated using the formula H = (D − d)/2, where H represents the inhibition zone in millimeters, D is the combined diameter of the sample and inhibition zone in millimeters, and d is the diameter of the sample in millimeters. Following the measurement of the inhibition zone, the specimens were carefully removed from the agar using a pair of tweezers.

RESULTS AND DISCUSSION

Structure of the ZnO nanoparticles

X-ray diffraction (XRD) analysis was employed to elucidate the composition and structural characteristics of ZnO films that had been deposited onto Ti6Al4V substrates. In essence, the X-ray diffraction patterns exhibited discernible diffraction lines, which unequivocally corresponded

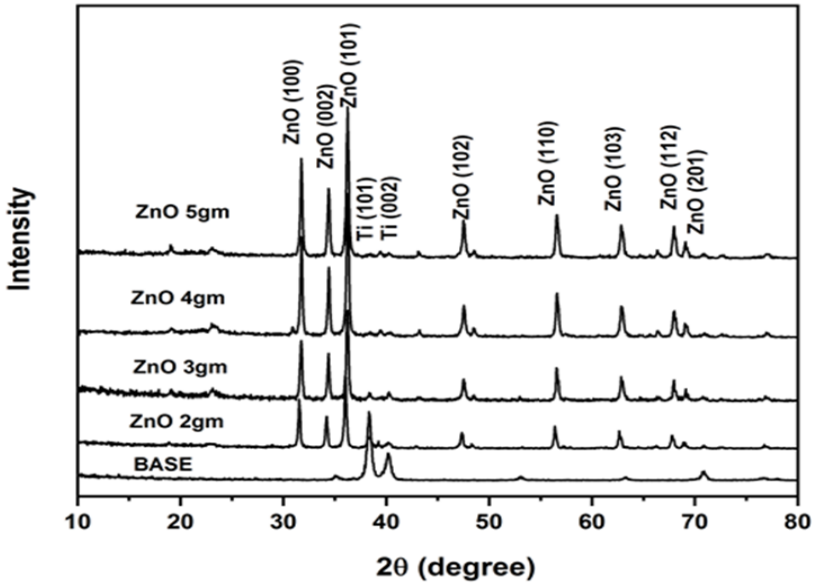

Fig. 1. XRD patterns for uncoated Ti6Al4V and coated samples with ZnO with different suspension concentrations.

to the ZnO phase (as per the ICDD file 36-1451). Additionally, traces of the Ti phase (according to the ICDD file 44-1494) were discerned (Fig. 1, 2, 3). The XRD patterns of the deposits, generated at varying concentrations of ZnO nanoparticles (2, 3, 4, and 5 g), voltage settings (10, 30, 50 Volts), and inter-electrode distances (1, 3, 5cm), consistently demonstrated the presence of polycrystalline

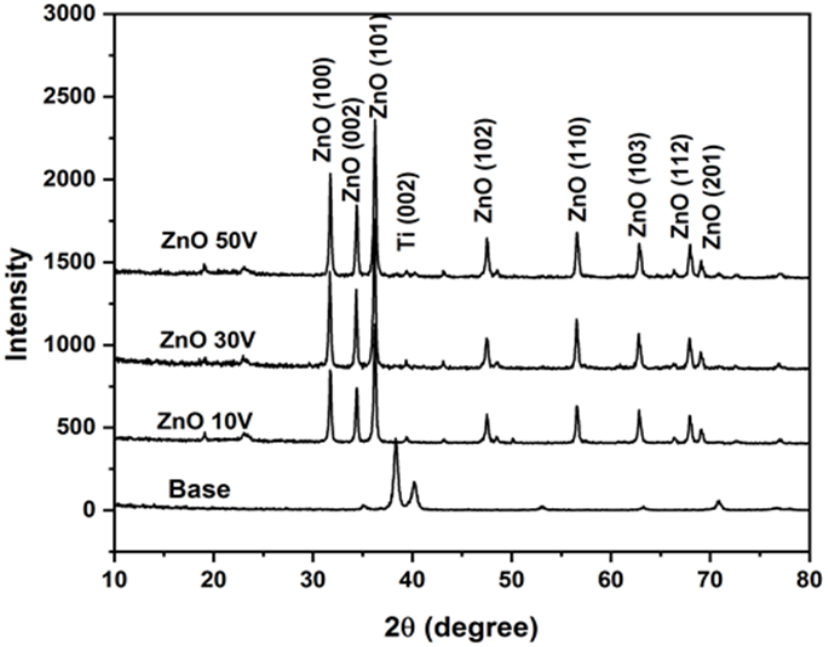

Fig. 2. XRD patterns for uncoated Ti6Al4V and coated samples with ZnO with different applied voltages.

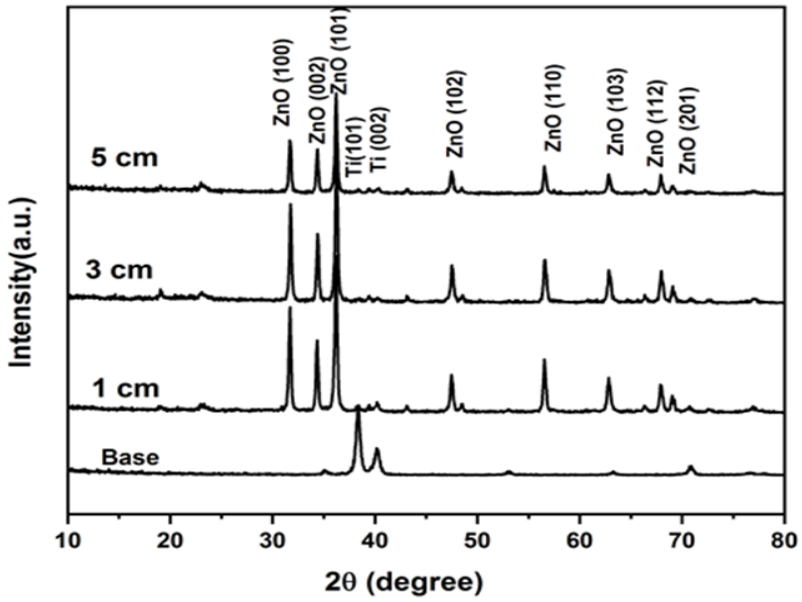

Fig. 3. XRD pattern for uncoated and Ti6Al4V coated samples with ZnO with different inter electrode spacings.

phases and prominent diffraction lines associated with ZnO. Notably, there were no discernible alterations in the crystal structure in comparison to the uncoated alloy. Only the diffraction peaks attributable to Ti were observed, specifically at angles θ = 38.42º and 40.17º, corresponding to the (002) and (101) planes of titanium. Other alloy constituents remained inconspicuous in the diffraction pattern, primarily due to their lower proportion within the alloy, rendering them less amenable to X-ray refraction. The X-ray diffraction analysis effectively unveiled the characteristic diffraction peaks that can be ascribed to the well-defined hexagonal wurtzite structure of ZnO. Utilizing Scherrer's equation [29], the average size of the ZnO crystallites was calculated and is presented in Table 1. Notably, when the XRD patterns were examined for the deposit produced at 50 V, a ZnO concentration of 5 mg, and an inter-electrode distance of 1 cm, all for a duration of 5 minutes, robust diffraction lines corresponding to ZnO were evident. This observation aligns with the expectation that the quantity of deposited ZnO exhibits an almost linear increase with escalating concentrations of nano-sized ZnO, and furthermore, the rate of ZnO deposit formation is positively correlated with augmented applied voltages. These findings are corroborated by

Table 1. the crystallite size of ZnO coating on Ti6Al4V, coated sample with different suspension concentration, with different applied voltage, and with different inter electrode spacing.

	2 g, 50 V, 1 cm			3 g, 50 V, 1 cm	
2θ(degree)	FWHM(degree)	C.S.nm	2θ(degree)	FWHM(degree)	C.S.nm
31.71	0.26	31.8	31.74	0.24	34.3
34.37	0.24	34.50	34.40	0.20	41.58
36.20	0.26	32.15	36.24	0.24	35.57
47.50	0.31	27.73	47.52	0.21	41.33
56.55	0.24	37.74	56.59	0.19	47.74
62.80	0.26	35.80	62.88	0.27	34.74
67.90	0.26	36.83	67.98	0.19	51.24
69.06	0.25	38.27	69.11	0.17	56.41
	4 g, 50 V, 1 cm			5 g, 50 V, 1 cm	
2θ(degree)	FWHM(degree)	C.S.nm	2θ(degree)	FWHM(degree)	C.S.nm
31.77	0.24	34.4	31.77	0.25	32.5
34.43	0.21	39.98	34.42	0.26	32.24
36.26	0.25	33.98	36.25	0.27	30.73
47.55	0.25	34.86	47.53	0.26	33.64
56.61	0.24	37.13	56.58	0.28	32.69
62.88	0.27	34.36	62.86	0.31	30.23
67.97	0.27	35.62	67.94	0.29	33.26
69.11	0.28	34.82	69.07	0.26	37.38
	5 g, 10 V, 1 cm			5 g, 30 V, 1 cm	
2θ(degree)	FWHM(degree)	C.S.nm	2θ(degree)	FWHM(degree)	C.S.nm
31.72	0.26	31.8	31.76	0.25	32.9
34.37	0.24	34.50	34.41	0.25	33.53
36.20	0.26	32.15	36.24	0.27	31.54
47.50	0.31	27.73	47.53	0.28	30.78
56.55	0.24	37.74	56.59	0.26	35.11
67.80	0.26	36.81	62.85	0.25	36.65
67.90	0.26	36.83	67.95	0.26	36.85
69.06	0.25	38.27	69.09	0.25	38.89
	5 g, 50 V, 3 cm			5 g, 50 V, 5 cm	
2θ(degree)	FWHM(degree)	C.S.nm	2θ(degree)	FWHM(degree)	C.S.nm
31.72	0.30	27.7	31.71	0.27	31.2
34.38	0.21	38.86	34.36	0.26	32.36
36.21	0.23	36.03	36.19	0.27	30.73
47.48	0.29	29.62	47.48	0.28	31.44
56.57	0.24	37.90	56.55	0.26	34.83
62.82	0.22	42.50	62.82	0.33	28.38
67.92	0.23	42.57	67.91	0.28	34.33
69.04	0.23	41.56	69.02	0.24	40.00

existing literature [30].

AFM Image Analysis

In Fig. 4, we present Atomic Force Microscope (AFM) images depicting both uncoated Ti6Al4V alloy samples and ZnO-coated samples, where variations in suspension concentration, applied voltage, and inter-electrode spacing are observed. Complementary data, including grain sizes of the ZnO thin films (ranging from 42.20 to 102.7 nm) and root mean square (RMS) roughness values (ranging from 14.82 to 44.10 nm), are tabulated in Table 2. These findings collectively underscore the marked heterogeneity in size and shape exhibited by the deposited films. As discerned from the visual representations, elevating the concentration of ZnO nanoparticles (at 5mg), applying a voltage of 50 Volts, and reducing the inter-electrode

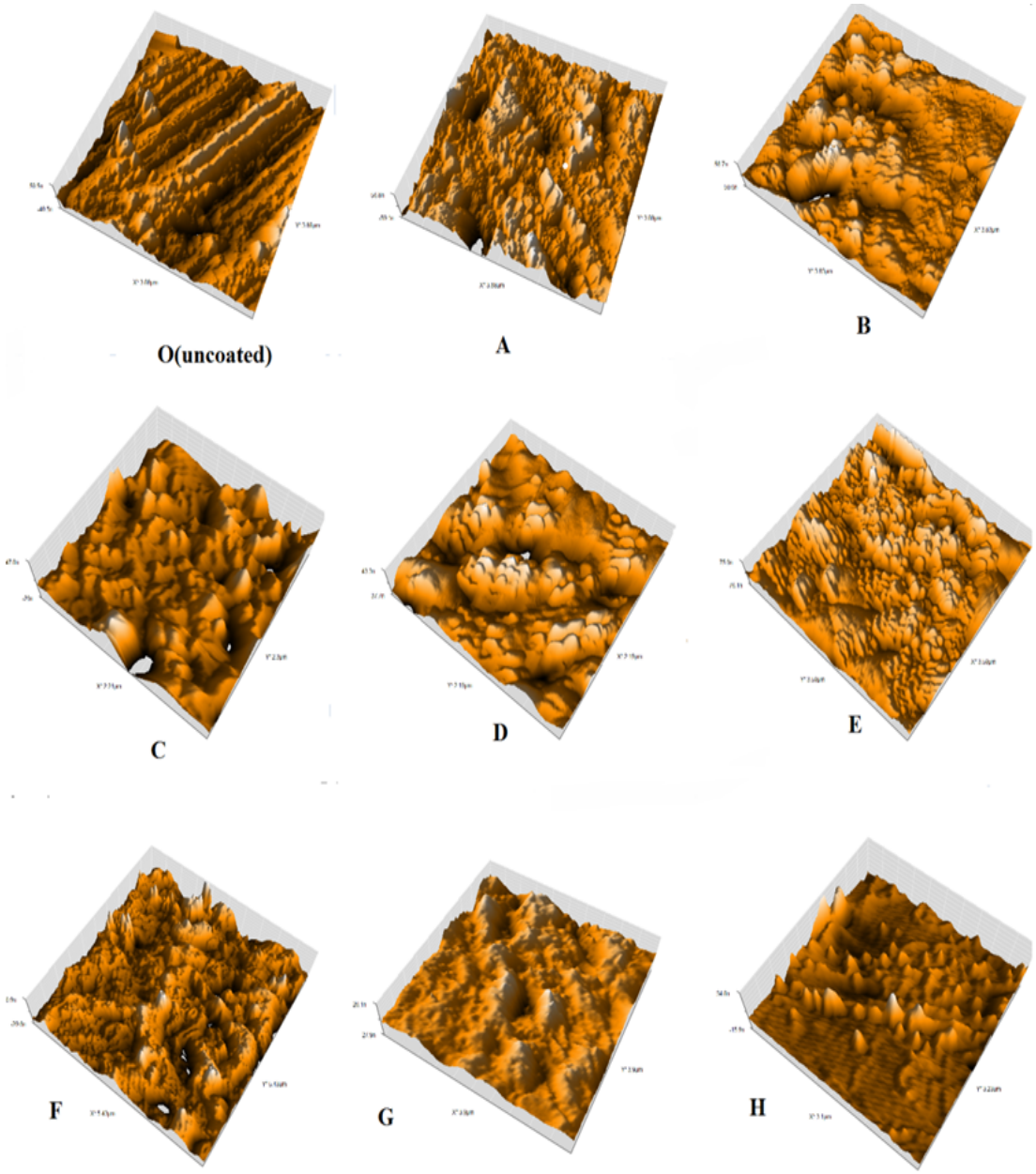

Fig. 4. Images of the optical microscope of (O) uncoated Ti6Al4V, (A, B, C) coated sample with different suspension concentrations, (D, E, F) with different applied voltages, (c) with different inter electrode spacings.

Table 2. Surface profile parameters of uncoated Ti6Al4V, (A, B, C) coated sample with different suspension concentrations, (D, E, F) applied voltages, (D, G, H) inter electrode spacings

Symbol	Preparation conditions of samples	Number of particle	Root mean square height (nm	Maximum height(nm)	Roughness (nm)	Grain size (nm)
O	Control(uncoated)	229	19.13	122.7	15.57	139.2
A	1g,50V,1cm	88	28.16	212.9	22.10	49.24
B	3g,50V,1cm	244	38.50	257.6	30.96	42.96
C	4g,50V,1cm	76	35.47	258.6	28.52	73.63
D	5g,50V,1cm	97	44.10	305.4	35.48	42.99
E	5g,10V,1cm	40	27.09	222.2	20.90	102.7
F	5g,30V,1cm	574	14.82	132.7	11.20	78.41
G	5g,50V,3cm	988	35.66	266.6	29.41	42.20
H	5g,50V,5cm	64	36.12	305.5	25.37	71.39

spacing to 1 cm led to an enlargement in grain size. This phenomenon is likely attributed to an accelerated deposition rate and the plausible agglomeration of smaller grains into larger ones. In instances where the lowest applied deposition voltage is employed, the ZnO film's morphology reveals a uniform layer with a random orientation, stemming from the presence of only a few grains characterized by an oriented texture (Fig. 4A). Notably, the surface exhibits an evident increase in roughness, with grain boundaries becoming more pronounced. The increase in grain size becomes more evident, accompanied by an augmentation in grain protrusions. Remarkably, surface porosity diminishes substantially, rendering the structure relatively discrete, with discernible deep valleys. The grain boundaries become distinctly delineated, and individual grains manifest as distinct microregions, each characterized by unique dimensions.

Conversely, the electrophoretic current exhibits an upward trend with increasing applied voltage, corresponding to greater deposition thickness. The associated increase in surface roughness is attributed to the migration of charged particles under the influence of the applied voltage. As the applied field strength amplifies, so does the force acting upon the particle, thereby augmenting the surface roughness of the film. Furthermore, as the suspension concentration of nano-sized ZnO escalates, the surface morphologies reveal the emergence of grain features on the film surface, manifesting with greater intensity. This phenomenon culminates in the formation of considerably larger grains within the ZnO films (Fig. 4B-H). This development is a consequence of enhanced surface mobility of adatoms, which are vital for the formation of continuous films. The intensified surface diffusion of these adatoms is facilitated by the elevated applied voltage, thus imparting momentum to the growing surface. Conversely, a higher suspension concentration of ZnO nanoparticles, coupled with elevated deposition voltage and reduced inter-electrode

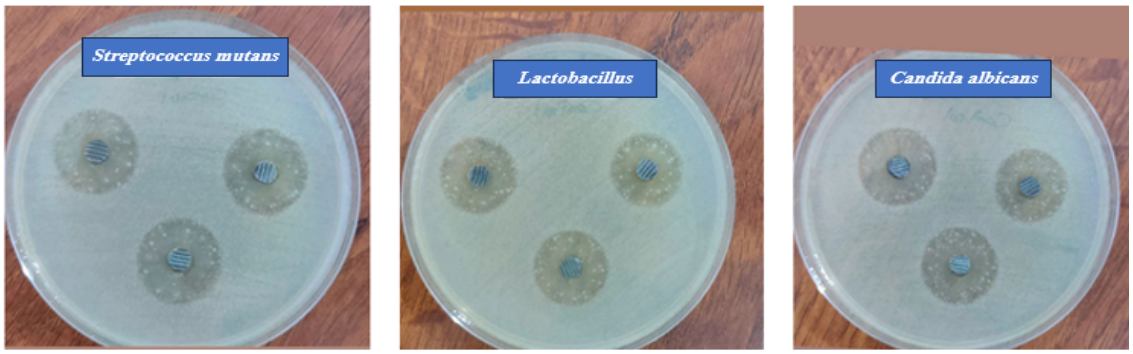

Fig. 5. antibacterial activity of Ti6Al4V samples against *Lactobacillus, Streptococcus mutans* and *Candida albicans*

spacing, yields an increase in RMS roughness due to the prominence of larger grains. This observed trend in RMS roughness corresponds directly with the crystallite size data (Table 2).

Antimicrobial Activity of ZnO Nanoparticles

As depicted in Fig. 5 and 6, the influence of ZnO nanoparticles on the growth of microorganisms, such as *Lactobacillus*, *Streptococcus mutans*, and *Candida albicans*, exhibits variability in its effects. The findings reveal that smaller ZnO nanoparticles exert a more pronounced impact on microbial cells, with *Lactobacillus* and *Streptococcus mutans* displaying greater susceptibility compared to *Candidan albicans*. ZnO nanoparticles achieve this by disrupting the structural integrity of the cell membrane and impeding the normal budding process, thereby impeding the growth of *Candida albicans*. Nonetheless, the efficacy of this mechanism varies depending on the specific microorganism, chiefly due to disparities in cell wall thickness [31]. Tables 3 and 4 compile the results of experiments where ZnO nanoparticle-coated and uncoated specimens were introduced into microbial cultures at specified intervals. After 24 hours of exposure, the observable effect was quantified and recorded as an inhibition zone. Notably, smaller grain sizes are correlated with increased active or specific surface area, facilitating enhanced interaction and penetration of microbial cell membranes, consequently heightening their antimicrobial activity. The results indicate that ZnO nanoparticles exhibit relatively greater effectiveness against *Lactobacillus* and *Streptococcus mutans* in contrast to *Candida albicans*, an outcome attributed to variations

Table 3. The mean inhibition zone of nanoparticles for Ti6Al4V samples against *Lactobacillus*, *Streptococcus mutans*, and *Candida albicans*.

Microorganism	The mean inhibition zone (mm)
Lactobacillus bacteria	10.66±1.15
Streptococcus mutans bacteria	9.66±0.57
Candida albicans	10±0

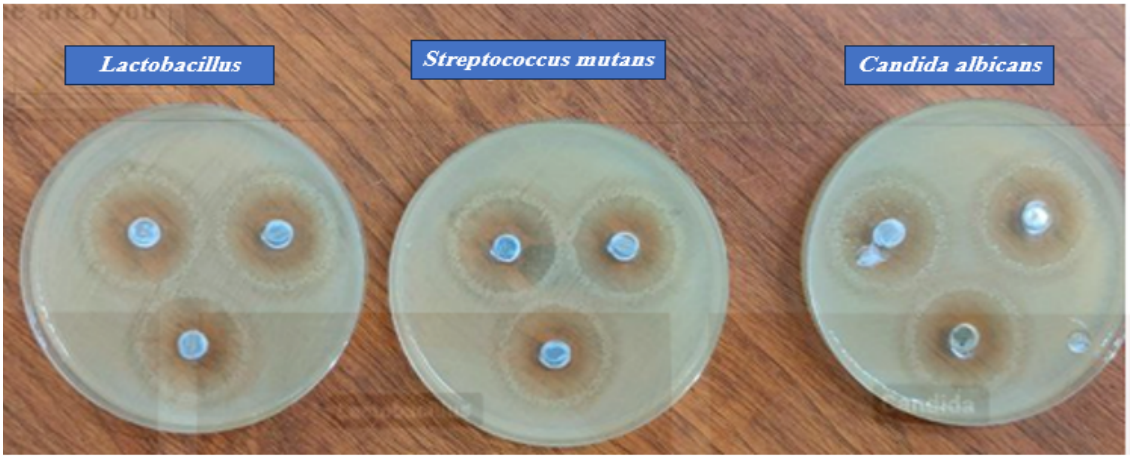

Fig. 6. antibacterial activity of ZnO nanoparticles film coated Ti6Al4V samples against *Lactobacillus*, *streptococcus mutans*, and *Candida*.

Table 4. The mean inhibition zone of nanoparticles for ZnO nanoparticles film coated Ti6Al4V samples against *Lactobacillus, Streptococcus mutans,* and *Candida albicans*

Microorganism	The mean of Inhibition zone (mm)
Lactobacillus bacteria	19±1
Streptococcus mutans bacteria	18±0
Candida albicans	17±1

in cell wall thickness. ZnO nanoparticles within the film potentially manifest antifungal activity by perturbing the structural integrity of the cell membrane and impeding the typical budding process. Differing degrees of sensitivity among microorganisms are likely due to disparities in

Table 5. Tests of normality

Vars.	Groups	Shapiro-Wilk		
		Statistic	df	p value
Streptococcus mutans	Control	0.955	10	0.732
	EPD	0.855	10	0.056
Lactobacilli	Control	0.860	10	0.059
	EPD	0.932	10	0.466
Candida albicans	Control	0.953	10	0.703
	EPD	0.940	10	0.550

Table 6. Descriptive and statistical test of diffusion inhibition zone among groups.

Groups		*Streptococcus mutans*	*Lactobacilli*	*Candida albicans*
Control	Min.	7.000	10.000	8.000
	Max.	12.000	12.000	12.000
	Mean	9.600	10.900	10.000
	±SD	1.430	0.994	1.155
EPD	Min.	16.000	17.000	15.000
	Max.	19.500	21.000	19.000
	Mean	18.000	19.300	17.000
	±SD	0.913	1.337	1.247
T test		15.659	15.938	13.024
P value		0.000	0.000	0.000

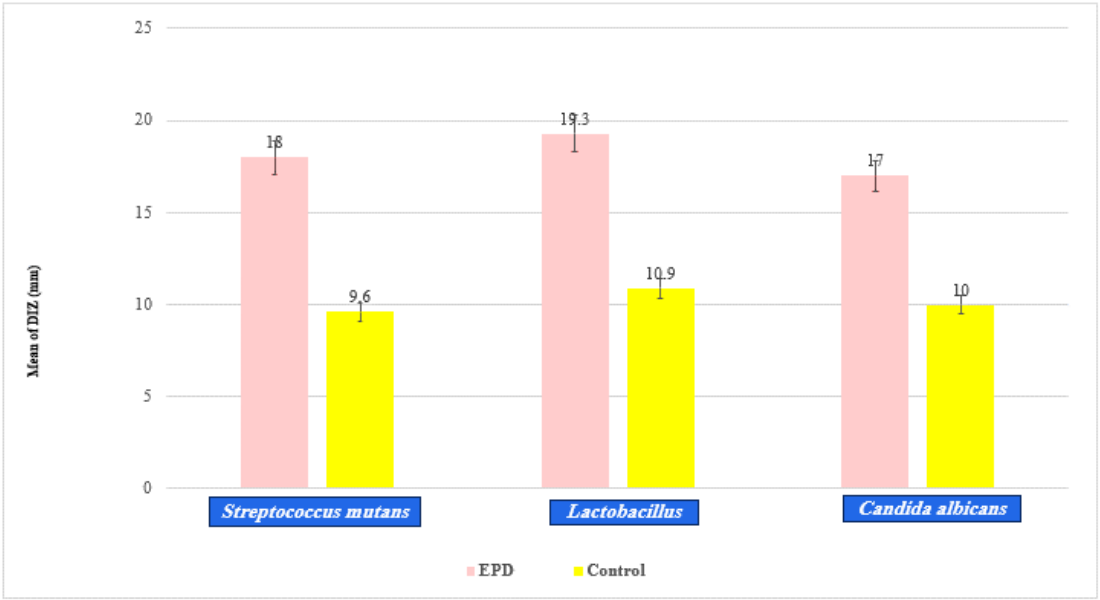

Fig. 7. cluster chart bar for inhibition zone

the structure and/or composition of their cell walls and extracellular matrices. This study posits the possibility that nanoparticles may adhere to bacterial cell walls and subsequently infiltrate them, ultimately leading to cell demise or the generation of free silver nanoparticle radicals capable of inflicting damage to the cell membrane. While the precise mechanism underlying antimicrobial activity remains incompletely understood, these findings are consistent with earlier research endeavors, aligning with prior investigations [31-37].

In an academic context, ZnO nanoparticle-coated Ti6Al4V samples exhibited noteworthy antimicrobial effectiveness against *Lactobacillus*, *Streptococcus mutans*, and *Candida albicans*, as determined through the Shapiro Wilk test at a significance level of $p>0.05$. The results presented in Table 5 indicate that the diameter of the inhibition zones for all microorganisms, in both the control group (uncoated Ti6Al4V) and the group with electrophoretic deposited (EPD) ZnO on Ti6Al4V samples follows a normal distribution. Data description, analysis, and presentation were conducted using the Statistical Package for Social Science (SPSS version 22, Chicago, Illinois, USA), as detailed in Table 6. Fig. 7 presents a cluster chart displaying key parameters, including minimum, maximum, mean, standard deviation, Shapiro Wilk test for normality, and Student T test. Significance was established when the p-value was less than 0.05. The application of ZnO-coated Ti6Al4V demonstrates considerable potential as a method to enhance antimicrobial efficacy against lactobacillus, *Streptococcus mutans*, and *Candida albicans*.

CONCLUSION

The current research reveals that the application of cathodic Electrophoretic Deposition (EPD) in an aqueous environment using a zinc anode is an effective and efficient technique for the formation of uniform, densely packed nanostructures exhibiting enhanced sintering properties, even at lower direct current (dc) voltage levels. The EPD process successfully facilitated the coating of the Ti6Al4V alloy surface with a zinc oxide (ZnO) phase, the characteristics of which were significantly influenced by the chosen deposition parameters. Optimal conditions for creating a homogenous and continuous ZnO layer were established at 50 volts, with a 5 mg concentration of ZnO nanoparticles and a 1 cm electrode gap. Additionally, the methodology employed for the synthesis of ZnO nanoparticles (ZnONPs) in this study was notably straightforward and economical. This approach not only simplifies the production process but also makes it more cost-effective. The synthesized ZnONPs solution demonstrated in this research exhibits promising potential as an effective agent for antibacterial and antifungal applications. This suggests its viability for use in a range of applications, particularly in enhancing the antimicrobial properties of materials used in medical and dental fields.

CONFLICT OF INTEREST

The authors declare that there is no conflict of interests regarding the publication of this manuscript.

REFERENCES

1. Curto A, Albaladejo A, Montero J, Alvarado A. Influence of a Lubricating Gel (Orthospeed®) on Pain and Oral Health-Related Quality of Life in Orthodontic Patients during Initial Therapy with Conventional and Low-Friction Brackets: A Prospective Randomized Clinical Trial. Journal of clinical medicine. 2020;9(5):1474.
2. Al-Ali DA, Al Groosh D. The influence of fixed orthodontic retainer on oral microbiota. International Journal of Health Sciences. 2022:2214-2223.
3. Al-Musallam TA, Evans CA, Drummond JL, Matasa C, Wu CD. Antimicrobial properties of an orthodontic adhesive combined with cetylpyridinium chloride. Am J Orthod Dentofacial Orthop. 2006;129(2):245-251.
4. Safi IN, Hussein BM, Aljudy HJ, Tukmachi MS. Effects of long durations of RF–magnetron sputtering deposition of hydroxyapatite on titanium dental implants. European Journal of Dentistry. 2021;03:440-447.
5. Wright M, Uddin A. Organic—inorganic hybrid solar cells: A comparative review. Sol Energy Mater Sol Cells. 2012;107:87-111.
6. Stanković A, Dimitrijević S, Uskoković D. Influence of size scale and morphology on antibacterial properties of ZnO powders hydrothemally synthesized using different surface stabilizing agents. Colloids Surf B Biointerfaces. 2013;102:21-28.
7. Sharma A, Ranjit R, Pratibha, Kumar N, Kumar M, Giri BS. Nanoparticles based nanosensors: Principles and their applications in active packaging for food quality and safety detection. Biochem Eng J. 2023;193:108861.
8. Hassan, S. A. H., Almaliki, M. N. S., Hussein, Z. A., Albehadili, H. M., Rabeea Banoon, S., Abboodi, A., Al-Saady, M. Development of Nanotechnology by Artificial Intelligence: A Comprehensive Review. Journal of Nanostructures, 2023; 13(4): 915-932.
9. Fouad O, Ismail A, Zaki Z, Mohamed R. Zinc oxide thin films prepared by thermal evaporation deposition and its photocatalytic activity. Applied Catalysis B: Environmental. 2006;62(1-2):144-149.

10. Barnes TM, Leaf J, Fry C, Wolden CA. Room temperature chemical vapor deposition of c-axis ZnO. Journal of Crystal Growth. 2005;274(3-4):412-417.
11. Yoo J, Lee J, Kim S, Yoon K, Park IJ, Dhungel SK, et al. High transmittance and low resistive ZnO:Al films for thin film solar cells. Thin Solid Films. 2005;480-481:213-217.
12. Escobedo Morales A, Herrera Zaldivar M, Pal U. Indium doping in nanostructured ZnO through low-temperature hydrothermal process. Optical Materials. 2006;29(1):100-104.
13. Yan Z, Song ZT, Liu WL, Wan Q, Zhang FM, Feng SL. Optical and electrical properties of p-type zinc oxide thin films synthesized by ion beam assisted deposition. Thin Solid Films. 2005;492(1-2):203-206.
14. Kim HY, Kim JH, Park MO, Im S. Photoelectric, stoichiometric and structural properties of n-ZnO film on p-Si. Thin Solid Films. 2001;398-399:93-98.
15. Fiddes AJC, Durose K, Brinkman AW, Woods J, Coates PD, Banister AJ. Preparation of ZnO films by spray pyrolysis. Journal of Crystal Growth. 1996;159(1-4):210-213.
16. Hara Y, Brownson JRS, Anderson MA. Fabrication of Thin-Films Composed of ZnO Nanorods Using Electrophoretic Deposition. International Journal of Applied Ceramic Technology. 2011;9(1):115-123.
17. Wong EM, Searson PC. Kinetics of Electrophoretic Deposition of Zinc Oxide Quantum Particle Thin Films. Chem Mater. 1999;11(8):1959-1961.
18. Tang F, Sakka Y, Uchikoshi T. Electrophoretic deposition of aqueous nano-sized zinc oxide suspensions on a zinc electrode. Materials Research Bulletin. 2003;38(2):207-212.
19. Tang F, Uchikoshi T, Sakka Y. Electrophoretic Deposition Behavior of Aqueous Nanosized Zinc Oxide Suspensions. J Am Ceram Soc. 2002;85(9):2161-2165.
20. Wang YC, Leu IC, Hon MH. Preparation and characterization of nanosized ZnO arrays by electrophoretic deposition. Journal of Crystal Growth. 2002;237-239:564-568.
21. Wang YC, Leu IC, Hon MH. Effect of colloid characteristics on the fabrication of ZnO nanowire arrays by electrophoretic deposition. Journal of Materials Chemistry. 2002;12(8):2439-2444.
22. Wu K, Zhitomirsky I. Electrophoretic Deposition of Ceramic Nanoparticles. International Journal of Applied Ceramic Technology. 2010;8(4):920-927.
23. Chen H-W, Lin C-Y, Lai Y-H, Chen J-G, Wang C-C, Hu C-W, et al. Electrophoretic deposition of ZnO film and its compression for a plastic based flexible dye-sensitized solar cell. Journal of Power Sources. 2011;196(10):4859-4864.
24. Yin X, Liu X, Wang L, Liu B. Electrophoretic deposition of ZnO photoanode for plastic dye-sensitized solar cells. Electrochem Commun. 2010;12(9):1241-1244.
25. Miao L, Cai S, Xiao Z. Preparation and characterization of nanostructured ZnO thin film by electrophoretic deposition from ZnO colloidal suspensions. Journal of Alloys and Compounds. 2010;490(1-2):422-426.
26. Lee J-H, Leu I-C, Chung Y-W, Hon M-H. Fabrication of ordered ZnO hierarchical structures controlled via surface charge in the electrophoretic deposition process. Nanotechnology. 2006;17(17):4445-4450.
27. Hamil M, Siyah M, Khalaf M. Electrophoretic deposition of Thin film TiO_2 on Ti6AL4V alloy surface for biomedical applications. Egyptian Journal of Chemistry. 2020;0(0):0-0.
28. khalaf m, saleh r, Hamil M. The Heat, Plasma, and Laser Treatments Characteristics of Hydroxyapatite Coatings. Egyptian Journal of Chemistry. 2021;0(0):0-0.
29. Lindley PF, Moss DS. Elements of X-ray crystallography by L. V. Azaroff. AcCrA. 1970;26(6):701-701.
30. Besra L, Liu M. A review on fundamentals and applications of electrophoretic deposition (EPD). Progress in Materials Science. 2007;52(1):1-61.
31. Lok C-N, Ho C-M, Chen R, He Q-Y, Yu W-Y, Sun H, et al. Silver nanoparticles: partial oxidation and antibacterial activities. JBIC Journal of Biological Inorganic Chemistry. 2007;12(4):527-534.
32. D. Awad G, D. Awad I, K. Khalaf M, L. Alshami M. In vitro study of the antibacterial effect of plasma surface treatment using Argon gas on orthodontic stainless steel brackets against Streptococcus mutans and Lactobacillus acidophilus. Bionatura. 2022;7(2):1-8.
33. Halob AA, Gatea IH, Khalaf MK, Sabar AB. Biopreparation for antimicrobial material from mixture of nano silver and olive leaves extract. IOP Conference Series: Materials Science and Engineering. 2020;928(6):062008.
34. Khalaf MK, Jebur E, Oraibi NS, Al-Taay HF. Influence of plasma sputtering pressure on the grain size of silver nanograins and their pathogenic bacteria inhibition. Annals of Tropical Medicine and Public Health. 2020;23(12).
35. Morones JR, Elechiguerra JL, Camacho A, Holt K, Kouri JB, Ramírez JT, Yacaman MJ. The bactericidal effect of silver nanoparticles. Nanotechnology. 2005;16(10):2346-2353.
36. Hailan SY, Al-Khatieeb MM. Antimicrobial efficacy of silver, zinc oxide, and titanium dioxide nanoparticles incorporated in orthodontic bonding agent. Journal of Baghdad College of Dentistry. 2019;31(3):10-16.
37. Jasim HM, Al-Dabagh DA, Mahmood MAA. Effect of different bracket types on streptococcus mutans count in orthodontic patients using fluoridated toothpaste. Journal of Baghdad College of Dentistry. 2020;32(2):1-4.